Appl Phys B (2010) 98: 593–600
DOI 10.1007/s00340-009-3798-z

Applied Physics B
Lasers and Optics

Detection of C_2H_2 and HCl using mid-infrared degenerate four-wave mixing with stable beam alignment: towards practical in situ sensing of trace molecular species

Z.W. Sun · Z.S. Li · B. Li · M. Aldén · P. Ewart

Received: 5 June 2009 / Revised version: 24 September 2009 / Published online: 1 November 2009

Abstract A stable and convenient optical system to realize the forward phase-matching geometry for degenerate four-wave mixing (DFWM) is demonstrated in the mid-infrared spectral region by measuring DFWM signals generated in acetylene (C_2H_2) and hydrogen chloride (HCl) molecules by probing the fundamental ro-vibrational transitions. IR laser pulses tunable from 2900 cm^{-1} to 3350 cm^{-1} with a 0.025 cm^{-1} linewidth were obtained using a laser system composed of an injection seeded Nd:YAG laser, a dye laser, and a frequency mixing unit. At room temperature and atmospheric pressure, a detection limit of 35 ppm ($\sim 9.5 \times 10^{14}$ molecules/cm^3) for C_2H_2 was achieved in a gas flow of a C_2H_2/N_2 mixture by scanning the P(11) line of the $(010(11)^0)$–(0000^00^0) band. The detection limit of the HCl molecule was measured to be 25 ppm ($\sim 6.8 \times 10^{14}$ molecules/cm^3) in the same environment by probing the R(4) line. The dependences of signal intensities on molecular concentrations and laser pulse energies were demonstrated using C_2H_2 as the target species. The variations of the signal line shapes with changes in the buffer gas pressures and laser intensities were recorded and analyzed. The experimental setup demonstrated in this work facilitates the practical implementation of in situ, sensitive molecular species sensing with species-specific, spatial and temporal resolution in the spectral region of 2.7–3.3 μm (3000–3700 in cm^{-1}), where various molecular species important in combustion have absorption bands.

PACS 78.47.nj · 33.20.Ea · 82.80.Gk

1 Introduction

Degenerate four-wave mixing (DFWM) is a comparatively mature laser-based diagnostic technique for the detection of trace molecular species with high sensitivity. As a coherent nonlinear method, the DFWM signal is generated as a highly collimated beam which enables remote and zero background measurements, while keeping the merits of laser-based diagnostic techniques, such as nonintrusive detection, high temporal and spatial resolution, together with species and quantum state selectivity. Since the first experimental demonstration of the detection of trace atomic [1] and molecular species [2] relevant to combustion more than 20 years ago, DFWM has been successfully applied to detect various transient and stable species by probing strong electronic transitions. Such transitions were mainly probed in the UV/visible spectral regions due partly to the relatively strong electronic transitions in these regions and partly to the availability of suitable laser sources and the comparatively easy optical arrangements. Comprehensive reviews of DFWM spectroscopy and its diagnostic applications can be found in references [3–6].

Compared with the large number of investigations in the UV/visible spectral regions, only a few applications of DFWM have been carried out in the mid-infrared spectral region by probing molecular ro-vibrational transitions. IR-DFWM detection of HF has been demonstrated by Vanderwal et al. by probing the (1–0) vibrational transition

Z.W. Sun · Z.S. Li (✉) · B. Li · M. Aldén
Division of Combustion Physics, Lund University, Box 118, 221 00 Lund, Sweden
e-mail: zhongshan.li@forbrf.lth.se

P. Ewart
Department of Physics, Clarendon Laboratory, Oxford University, Parks Road, Oxford, OX1 3PU UK

near 4000 cm^{-1} [7]. Germann et al. detected HCl by probing the R(1) ro-vibrational transition with IR-DFWM at a pressure of 200 torr and determined the transition moment and concentration by multiplex spectroscopy [8]. CH_4 and C_2H_2 were investigated making use of C-H stretching ro-vibrational transitions near 3000 and 3300 cm^{-1}, respectively, and the results indicated that IR-DFWM was a sensitive diagnostics technique for polyatomic hydrocarbon molecules with a detection limit of $\sim 1.5 \times 10^{11}$ molecules/cm^3 per quantum state for 1 mtorr CH_4 gas in 3 torr N_2 buffer gas [9]. Similar investigations were performed by Voelkel et al.; in their work a detection limit of 2.4×10^{14} molecules/cm^3 was estimated for CH_4 at a total pressure of 5 mbar [10]. Also reported in the same work was a phenomenon that stimulated Raman scattering suppressed the IR-DFWM signal along the direction of the probe beam for CO_2 and N_2O molecules. Tang et al. applied IR-DFWM to measure jet-cooled C_2H_2 [11, 12]. It should be noted that all the DFWM measurements in the mid-infrared region mentioned above were performed at low pressures.

Two experimental configurations have been frequently used in DFWM spectroscopy, namely the phase-conjugate geometry (PCG) and the forward phase-matching geometry (FPG) [4, 13]. The PCG can be used to achieved sub-Doppler spectral resolution, while the FPG, similar to the folded BOXCARS arrangement in coherent anti-Stokes Raman scattering [14], has been proved to be more suitable to detect trace gaseous molecules for the following reasons. Firstly, in the FPG, the signal beam is easier to isolate from the other three input beams due to nonspatial overlap, and can avoid the interference from stimulated Raman scattering when some molecules are measured using a stronger probe beam. Secondly, because the same Doppler shift is experienced for each of the three input beams, all molecules within the Maxwell-Boltzmann distribution contribute to the signal. This results in a greater efficiency than that in the case of the PCG, where only the zero-velocity subgroup couples to the laser fields. In addition, the three input beams go through nearly the same optical path, so that the beam steering effect is greatly reduced in turbulent and high-pressure environments. Besides the merits and drawbacks mentioned above, in the mid-infrared spectral region both geometries face the difficulty of aligning three invisible beams so that they overlap in the interaction region to ensure proper phase matching. This experimental difficulty has probably formed the major hindrance to practical applications of DFWM in the mid-infrared region. Meanwhile polarization spectroscopy (PS) has been developed in the mid-infrared in order to overcome this difficulty. In a PS setup, the overlap of only two beams, the pump and the probe beams, are required. Furthermore, the position of the signal beam in the far field can be exactly located by the probe beam by slightly uncrossing the polarizer in the signal detection path. Facilitated by these practical advantages, IRPS has been successfully applied to detect OH [15], CO_2 [16–18], H_2O [15, 17], HCl [19], and several polyatomic hydrocarbon molecules, e.g., C_2H_2 [20], CH_4, and C_2H_6 [21] in cold gas flows and flames at atmospheric or lower pressures. IRPS, however, relies heavily on high quality polarizers and suffers from difficulties when the sample to be measured is contained in a cell owing to stress-induced birefringence in the windows. More recently IR-DFWM using the PCG has been compared to IRPS for the detection of CH_4 [22].

In order to improve the practicality of IR-DFWM, the problem of reliably achieving accurate overlap of the pump and probe beams is addressed in the present work. To this end a device to produce the required beam geometry, termed IR-BOXCARS plates, has been designed for use in the mid-IR spectral range, similar to the one demonstrated previously [23, 24] in the UV, where NO molecules were detected around 226 nm. In this device, a pair of specially coated parallel-sided optical plates were designed to conveniently produce four parallel propagating beams of approximately equal intensities. Three of these beams are easily crossed using a focusing lens to produce the IR-DFWM signal. Using this system the laser beams are automatically phase-matched and the signal beam can be easily located by using the fourth beam, which follows the signal path. The signal beam is also easily spatially filtered from the other three forward-going beams.

In this work, sensitive detection of trace levels of C_2H_2 and HCl molecules with IR-DFWM are demonstrated using the IR-BOXCARS device, which greatly facilitates the optical alignment in the mid-infrared region. As demonstration measurements, C_2H_2 and HCl mixed in a nitrogen gas flow were detected using IR-DFWM in the FPG geometry by probing the fundamental ro-vibrational transitions of the gases. High sensitivities were achieved; down to tens of parts per million for both species at room temperature and atmospheric pressure.

2 Experimental

A schematic of the experimental apparatus is shown in Fig. 1(a). The IR laser system is composed of a Nd:YAG laser, a dye laser, and a frequency mixing unit, which have been described in detail in a previous paper [15]. The IR laser pulses, tunable from 2900 cm^{-1} to 3350 cm^{-1} with a 0.025 cm^{-1} linewidth (measured using an excitation scan of IR laser-induced fluorescence of CO_2 over the P(24) line in a 10 mbar gas cell; see a previous work [17]), were traced by a HeNe laser beam in order to facilitate the beam alignment. After passing two apertures, the IR beam was split into four symmetrically distributed parallel beams with near equal energy by a beam splitter plate assembly (BP), which is described below. Three of the separated beams were brought

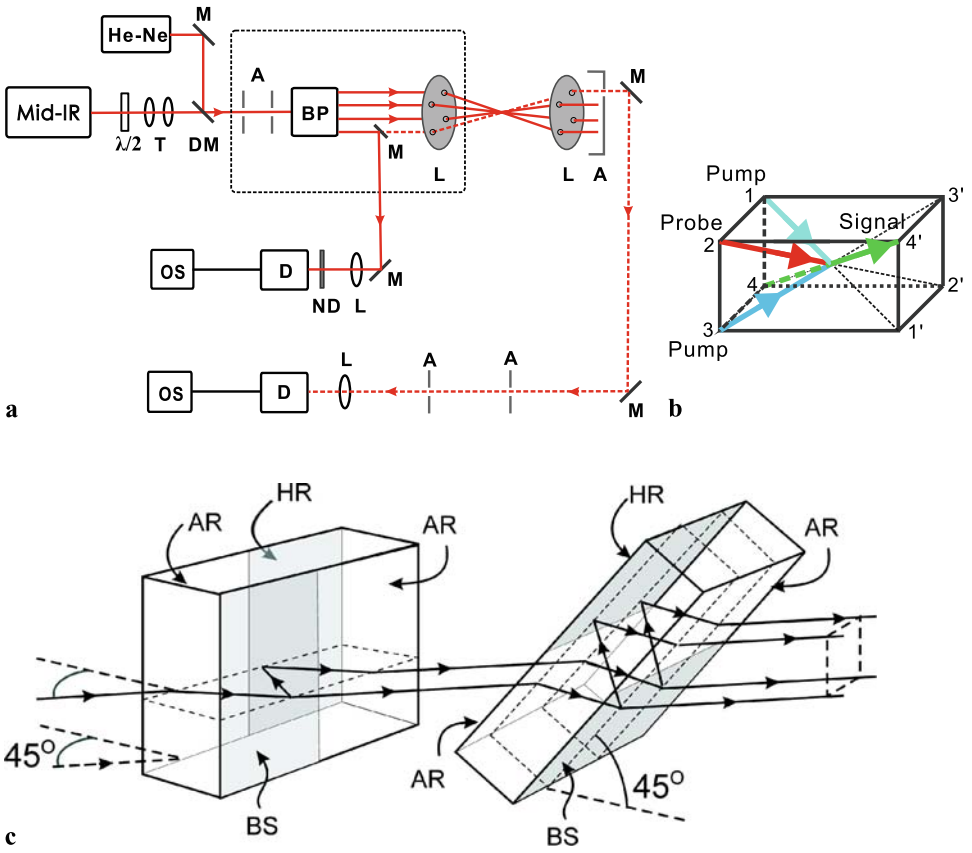

Fig. 1 (**a**) Schematic of the experimental setup. T, telescope; DM, dichroic mirror; M, mirror; A, aperture; BP, beam splitter plate assembly; L, CaF_2 lens; D, InSb detector; OS, oscilloscope and ND, neutral density filter. (**b**) Forward phase-matching geometry of DFWM. (**c**) Beam splitter plate assembly shown as BP in (**a**). AR, anti-reflection coating; BS, 50% reflection coating; HR, high reflection (>95%) coating; two beam splitters work together, oriented in orthogonal planes, in order to produce four parallel output beams. The beam incident from the left at 45° to the first plate is split into two parallel beams in a horizontal plane. Each of these two beams is split by the second plate into two parallel beams in the vertical plane, leading to four parallel beams arranged at the corners of a square and exiting at the right

to a common focus by an $f = 500$ mm CaF_2 lens to define the interrogated volume. This arrangement leads to the production of the DFWM signal beam in the forward phase-matched folded BOXCARS geometry shown in Fig. 1(b). The signal beam and the three input beams were collimated by another CaF_2 lens ($f = 500$ mm). The signal beam was then spatially filtered by three apertures and focused onto a liquid N_2-cooled InSb detector. The fourth beam from the BP was used to trace the signal beam since it copropagates with the signal owing to the phase-matching condition. Use of this fourth beam greatly facilitated the alignment of the signal beam onto the detector. During the signal generation process, this fourth beam was prevented from reaching the interaction regions and was reflected to another IR detector and used to record the laser energy fluctuations in real time.

The IR BP is composed of two identical parallel-sided plates similar to those used in previous work [23, 24], where their construction is described. For convenience the arrangement is described briefly here and is shown schematically in Fig. 1(c). The accurately parallel-sided plates are constructed from CaF_2 with dimensions $50 \times 50 \times 15$ mm^3 and coated with anti-reflecting, 50% reflecting, and high reflecting (>95%) layers over the areas shown in the diagram. The horizontally propagating single infrared input beam is incident on the first plate, which is tilted at an angle of 45°. The input and output facets are anti-reflection coated; the first internal reflection facet is coated to yield 50% reflection, and the second internal reflection facet is coated to yield high reflection. The coatings were prepared for the spectral range 2.7–3.3 μm (3000–3700 in cm^{-1}). One input beam is thus split into two parallel beams with almost equal intensities. Each beam is further split into two beams in the second identically prepared plate. This second plate is tilted by 45° about an axis perpendicular to that of the first plate. Fine adjustment of the angles of incidence on the BP around 45° results in four parallel beams distributed at four corners of a 12×12 mm rectangle with almost equal intensities. All the beams were focused to a common point with an $f = 500$ mm CaF_2 lens, giving an angle between pump and probe beam of about 1.4°. The probe volume in this setup was estimated to be $0.4 \times 0.4 \times 10$ mm^3 when the wavelength of the laser output was 3 μm. The total loss of laser energy due to reflections and transmissions through the BP is less than 15%. All the parts shown in Fig. 1(a) in the dashed-line box were installed on a separate optical board, and the two fixed apertures before the BP were designed to lock the direction of the input beam. This design substantially facilitates the alignment process, especially in the mid-infrared spectral range, where visible beam indicators are lacking.

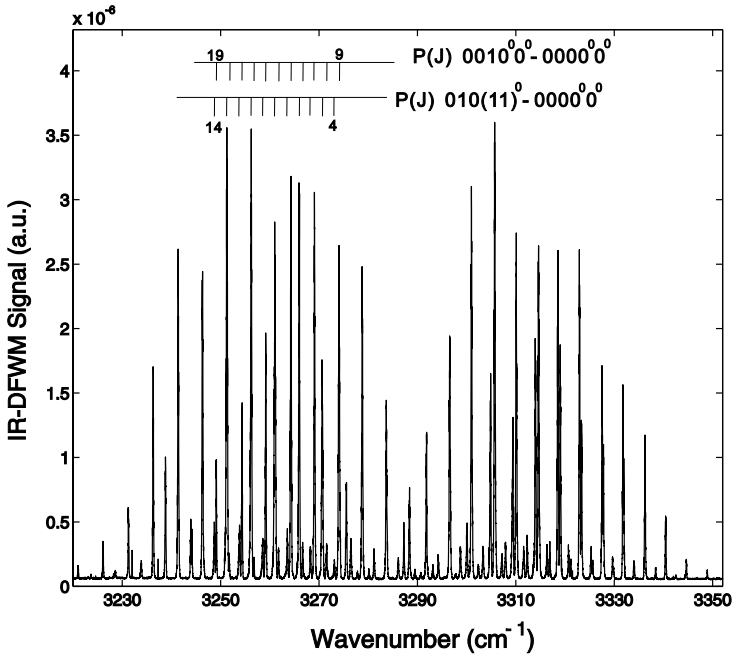

Fig. 2 IR-DFWM spectrum of 510 ppm C_2H_2 in a nitrogen gas flow. The laser energy was kept at ∼2.0 mJ/pulse, which is under the saturation condition. Line intensities have not been corrected for the laser intensity fluctuations. Partial assignments of the spectral lines have been made

3 Measurements and results

3.1 C_2H_2 measurements

Acetylene (C_2H_2) is both a common fuel in, and an intermediate product of, combustion and also plays an important role in soot [25] and polycyclic aromatic hydrocarbon formation [26, 27] in hydrocarbon combustion. Hence, this species has been studied using several spectroscopic techniques in different environments. With vibrational coherent anti-Stokes Raman scattering (CARS), Farrow et al. reported C_2H_2 measurement in an ethylene flame [28]. In a further study they demonstrated a detection limit of about 2000 ppm at 1000 K in an acetylene-doped flame [29]. Bood et al. used dual-broadband pure rotational CARS to analyze the rotational structure of C_2H_2 in a heated gas cell [30]. DFWM in the mid-IR spectral range has also been applied to C_2H_2 detection in a low-pressure chamber and a gas jet [9–11, 31]. Laser-induced fluorescence (LIF) around 228 nm [32] and spontaneous Raman scattering (SRS) [33] in flames were also reported. Li et al. performed C_2H_2 IRPS measurements in cold flow and in a 50 mbar methane/oxygen flame, and a detection sensitivity of 10 ppm in a 70 mbar gas mixture was achieved [20]. Chai et al. reported the detection of C_2H_2 at low concentrations by electronic resonance-enhanced CARS (ERE-CARS) at around 226 nm, and a detection limit of approximately 25 ppm at 300 K and 1 bar was achieved for their experimental conditions [34].

Owing to its importance in combustion and its well-known spectroscopic structure, C_2H_2 was chosen as the target species in our measurements to demonstrate the utility of the BP device for IR-DFWM. Shown in Fig. 2 is an excitation IR-DFWM spectrum which was obtained using the above-mentioned setup with a total pulse energy of ∼2 mJ for the two pump and the probe beams. The gas samples were prepared in a laminar flow on top of a sintered porous metal plug of 3 cm diameter. A commercial C_2H_2/N_2 (AGA, 1.99(4)% mole fraction of C_2H_2) gas mixture flow was further diluted by another N_2 flow. The gas flow was controlled by mass flow meters in order to produce gas mixtures with different C_2H_2 concentrations. Figure 2 shows a spectrum obtained when the concentration of C_2H_2 was 510 ppm ($\sim 1.4 \times 10^{16}$ molecules/cm^3). It should be noted that no correction of the line intensities due to the laser pulse energy fluctuations was performed. Spectral structures were recognized and partial assignments of the spectral lines were made according to Rinsland et al. [35]. Owing to power broadening and Doppler broadening, some lines are overlapped. However, the P(10) line from the $(010(11)^0)$–(0000^00^0) band and the P(15) line of the (0010^00^0)–(0000^00^0) band, with a frequency shift of 0.61 cm^{-1} [35], can be clearly resolved. In the spectrum shown in Fig. 2 the full width at half-maximum (FWHM) for isolated lines was estimated to be 0.18 cm^{-1} based on measurements of the P(11) line of the $(010(11)^0)$–(0000^00^0) band. This line was chosen for the investigations described below.

The power dependence of the IR-DFWM signal was investigated by varying the total laser pulse energy. Figure 3 shows the dependences of the line-integrated IR-DFWM signal intensities on the laser pulse energies. The IR-DFWM signals were collected from a gas mixture with 850 ppm C_2H_2 diluted with N_2 at atmospheric pressure. At the low energy range, the fitted line in Fig. 3 has a slope of ∼3.0,

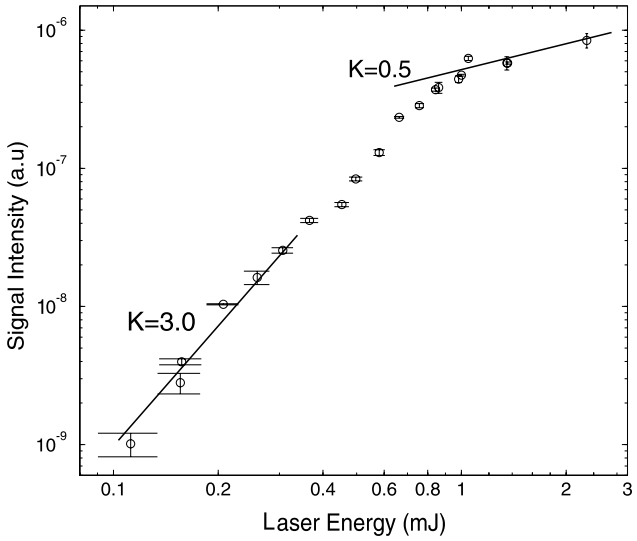

Fig. 3 Power dependence of the C_2H_2 IR-DFWM signal recorded in 850 ppm C_2H_2 in nitrogen. The measurements were based on the P(11) line of the $(010(11)^0)$–(0000^00^0) band. The laser energy shown was the sum of probe and pump beam energies

which agrees with previous investigations [36]; and at the high laser pulse energy range, the fitted line has a slope of ∼0.5, which indicates that saturation can be achieved in our measurements [36]. From Lucht et al. [37], the severe pressure dependence of the unsaturated DFWM signal can be considerably reduced by operation in the saturation regime.

High resolution excitation scans of the P(11) line of acetylene were performed in order to investigate the IR-DFWM line shapes, and the results are shown in Fig. 4. The partial IR-DFWM spectra shown in Fig. 4(a) and (b) were recorded at atmospheric pressure with the gas sample prepared in a laminar gas flow with about 150 ppm acetylene diluted with N_2. The laser pulse energy used in obtaining the spectra shown in Fig. 4(a) and (b) were 2.0 mJ and 0.2 mJ, respectively. The partial IR-DFWM spectrum shown in Fig. 4(c) was recorded at a pressure of 50 mbar with about 4000 ppm acetylene mixed with N_2. The low-pressure gas sample was prepared in a stainless steel chamber with two parallel sapphire windows. The laser pulse energy used in obtaining the spectrum in Fig. 4(c) was 0.2 mJ.

In general the determination of line shapes in DFWM is a complex matter. The line shape of DFWM using FPG in the presence of saturation was considered by Attal-Tretout and co-workers [38]. A comprehensive treatment of DFWM by direct numerical simulation has been presented by Lucht et al. [37] and applied specifically to the case of FPG [13] and to the calculation of saturation effects on line shapes in complex molecular spectra [39]. A nonperturbative analytical, and therefore less computationally expensive, treatment of DFWM developed by Bratfalean et al. [40] treated the case of saturation by pump and probe in the forward geometry—which is the situation encountered in the present work. This

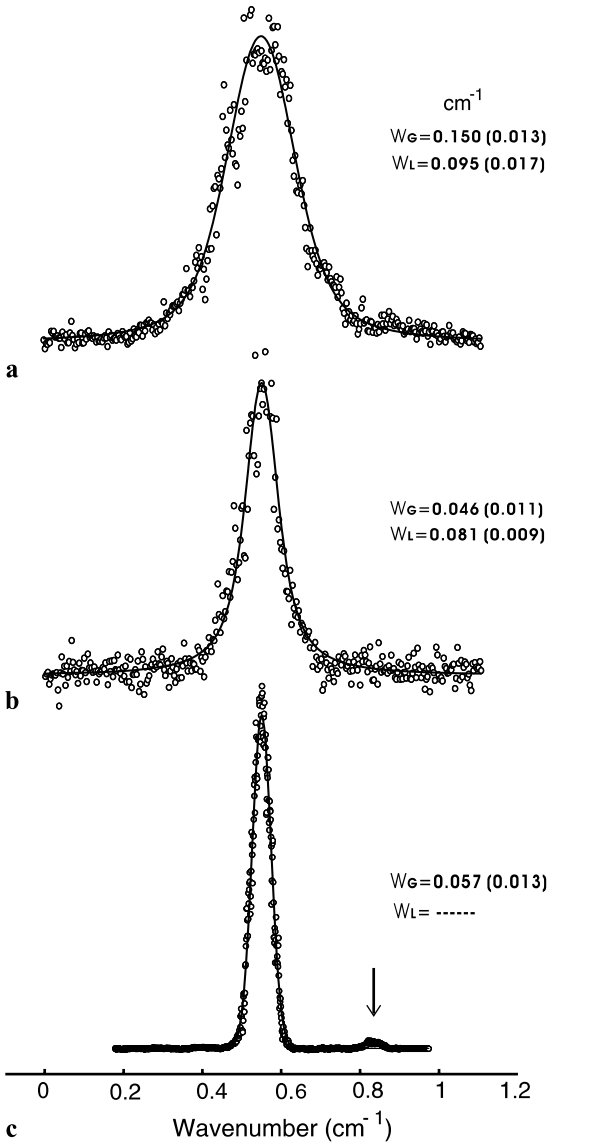

Fig. 4 IR-DFWM line shapes of the P(11) line at different laser energies and pressures. (**a**) $I = 2.0$ mJ and $P = 1$ bar, (**b**) $I = 0.20$ mJ and $P = 1$ bar, and (**c**) $I = 0.20$ mJ and $P = 50$ mbar. (**a**) and (**b**) were obtained at a concentration of 150 ppm C_2H_2, whereas (**c**) was measured at a concentration of 4000 ppm C_2H_2 in a low-pressure cell. The *circles* represent measured values, and the solid lines are fitted Voigt profiles. The weak signal line indicated by an *arrow* in (**c**) was attributed to the P(12) line of the isotope HCC(13)H

model was used to analyze saturation by both pump and probe fields since, as in the present work, optimum DFWM signals are optimized by using equal pump and probe intensities. The broadening effect caused by finite laser linewidth on the DFWM line shape has also been considered using a simplified model which neglects contributions of nondegenerate terms arising from different frequency components within the laser linewidth. The combined effect of power broadening and finite laser bandwidth on DFWM of complex molecular spectra including overlapping power broad-

ened lines has also been investigated [41]. Coherent interference effects from neighboring transitions may also lead to narrowing or broadening of the lines. In the present work many of the above factors will make a contribution to the observed line shape, but an empirical approach is adopted here to model the observed line shapes using Voigt profiles. The Voigt profile has been chosen since it appears to provide a good approximation to the observed line shapes within the experimental uncertainties.

In Fig. 4 the circles represent the measured data points, and the black solid lines present the best fitted Voigt profiles. The contributions from Gaussian and Lorentzian parts based on the fitting are also shown in the figures. It should be noted, however, that the laser spectrum was approximately Gaussian with a linewidth of 0.025 cm^{-1}, which is of the same order as the collisional and Doppler contributions. Consequently the sensitivity of the fit to the relative contributions of Lorentzian and Gaussian components is somewhat reduced. Nonetheless the data show that the shape and width of the lines are separately affected by collisional and power broadening.

From Fig. 4(a) and (b) one can see that at atmospheric pressure the Lorentzian contribution stays constant within the fitting uncertainties, while the line broadening mainly comes from the Gaussian contributions, which are 0.046 cm^{-1} and 0.150 cm^{-1} at low and high laser energies, respectively. The Lorentzian part can be ascribed to collisional broadening while the differences in the Gaussian part can be ascribed to power broadening, which includes saturation and ac Stark effects. The laser linewidth also contributes a Gaussian component. As indicated above, the effect of power broadening with finite bandwidth laser will be influenced by nondegenerate terms whose contribution is difficult to calculate under saturation conditions [41]. Given the experimental uncertainties in the present work, the effect of power broadening is modeled by a Gaussian contribution. In the absence of power broadening, the broadening due to collision effects is demonstrated in Fig. 4(b) and (c), where the signals have been generated with the same weak (unsaturating) laser power. At low pressure and weak laser energy, the line shape is close to a pure Gaussian profile, as shown in Fig. 4(c), which is consistent with the dominant effects being those of Doppler broadening and the laser linewidth. The Gaussian contribution stays constant within fitting uncertainties for different pressures, and the Lorentzian contribution becomes dominant when the pressure changes from 50 mbar to atmospheric pressure. The weak signal line indicated by an arrow in Fig. 4(c) is from the P(12) line of the isotope HCC(13)H, which can be seen clearly due to the high spectral resolution at low pressure. The measurements performed with the low-pressure cell also indicate that the IR-DFWM setup presented here can be used for measurements with windows, such as engines, where the IRPS technique could not be applied owing to stress-induced birefringence.

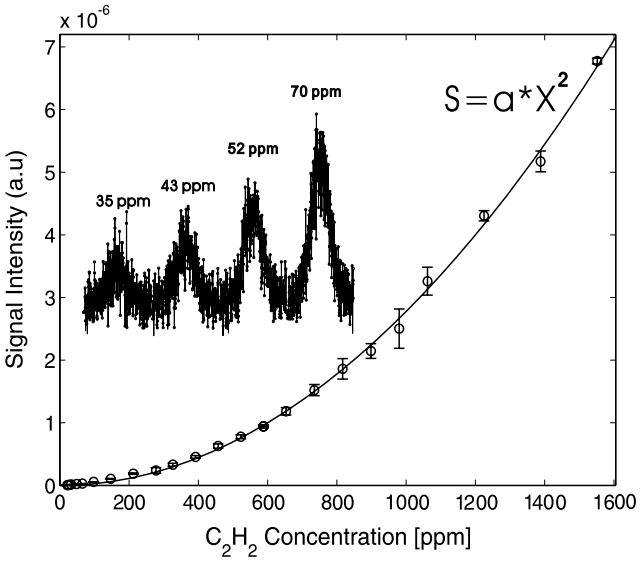

Fig. 5 IR-DFWM signal intensities for different C_2H_2 concentrations. The recorded signals for the four low concentrations are shown in the inset. The laser energy used was kept at ~2.0 mJ/pulse

The dependence of the IR-DFWM signal on the acetylene number densities was investigated, and Fig. 5 shows the line-integrated IR-DFWM signal intensities collected at different acetylene concentrations. The sample gas mixture was prepared in the laminar gas flow at atmospheric pressure with acetylene diluted by N_2. During the measurements, the laser pulse energy was kept at ~2.0 mJ to make sure that the saturation condition was fulfilled. Since under optically thin conditions the IR-DFWM intensity should have a simple quadratic relation with molecular number density regardless of saturation, a $S = a \cdot N^2$ relation was adopted to fit the signal-concentration curve as shown in Fig. 5, where a good fit in the concentration range (30–1600 ppm) was obtained. Moreover, the raw signals recorded during measurements of the last 4 data points of 35 ppm, 43 ppm, 52 ppm, and 70 ppm C_2H_2 concentrations are shown as the inset in Fig. 5. A detection sensitivity of 35 ppm ($\sim 9.5 \times 10^{14}$ molecules/cm^3) was estimated at atmospheric pressure for C_2H_2 based on the signal-to-noise ratio obtained. Furthermore, the squared dependence of signal intensities on concentrations makes IR-DFWM more sensitive to changes in the concentrations of the measured species.

3.2 HCl measurements

HCl is a particularly interesting chemical species due to the important roles it plays in various research areas, e.g., photochemistry [42], plasma etching [43], and bio-fuel combustion [44] as well as its toxic and corrosive effects in fire smoke [45]. Moreover, HCl is very reactive and frequently

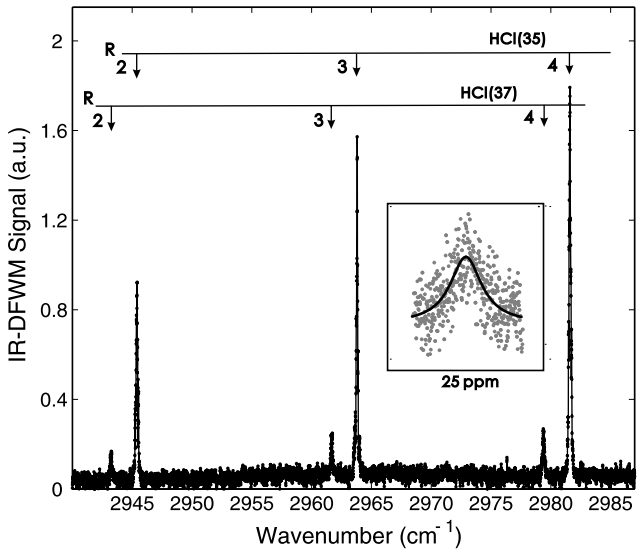

Fig. 6 IR-DFWM spectrum of 100 ppm HCl diluted in a nitrogen gas flow. The raw signal of HCl(35) R(4) line with a concentration of 25 ppm is shown as an *inset*

generated during many industrial processes, such as those used in waste incineration and aluminum plants. Approximately 90% of the Cl present in combustion processes will end up as HCl in the flue gas [46]. An understanding of the complex processes involving HCl will be aided by information provided by nonintrusive in situ measurements of key parameters using optical techniques. Generally tunable diode laser absorption spectroscopy is utilized for in situ HCl detection by probing the overtone vibration in the near-IR spectral region [43, 46], and recently Li et al. performed spatially resolved trace detection of HCl in flames with IRPS [19].

The IR-DFWM technique is applied in this work to detect HCl molecules at atmospheric pressure and room temperature. Shown in Fig. 6 is an excitation scan of HCl recorded in a laminar gas flow of a HCl/N_2 mixture with 100 ppm HCl, where the sample gases were prepared in the same way as for acetylene. The doublet structure due to the two isotopes of chlorine can be clearly identified in the spectrum. The R(4) line belonging to HCl(35) was chosen to check the sensitivity of IR-DFWM for HCl detection, and the raw spectrum of a gas sample with 25 ppm HCl mixed in N_2 is shown as an inset of Fig. 6. The detection sensitivity at atmospheric pressure and room temperature is estimated to be 25 ppm ($\sim 6.8 \times 10^{14}$ molecules/cm) based on the spectrum shown in Fig. 6.

3.3 Comparison of IR-DFWM and IRPS

Since both IR-DFWM and IRPS techniques are available in our laboratory, a direct comparison of the pros and cons of these twin nonlinear techniques for practical applications can be performed. This work complements the more qualitative comparison between IRPS and IR-DFWM in the PCG reported previously [22]. The sensitivity comparison between IR-DFWM and IRPS was experimentally performed for the HCl molecule by probing the R(4) line at room temperature and atmospheric pressure. A detailed description of the IRPS experimental setup used can be found in [15]. Using the IRPS technique a detection limit of 30 ppm was achieved, whereas by the IR-DFWM technique it was 25 ppm, as discussed in Sect. 3.2. The sensitivities of these twin nonlinear techniques are found to be much the same. It should be noted, however, that the measurements were not obtained under identical experimental conditions. Owing to the use of different lenses ($f = 500$ mm in DFWM and $f = 1000$ mm in PS) to focus the laser beams to measuring points and the different angles between pump beams and probe beam ($\theta = 1.4°$ in DFWM and $\theta = 3°$ in PS), the detection volumes ($\sim 0.4 \times 0.4 \times 10$ mm^3 in DFWM and $\sim 0.7 \times 0.7 \times 15$ mm^3 in PS) and the laser energy densities were different in each case. Even though the energies of laser output were controlled to be equal in the two techniques, the residual energies arriving at the detection volume were still different owing to different energy losses arising from the different components used in each experimental setup.

Besides sensitivity, another important factor in practice is the ease of implementation of the technique, for which the IR-DFWM setup described in this work has advantages over IRPS. The fewer optical components needed, easier alignment, lower cost, and higher stability, based on the comparisons in our laboratory, make the IR-DFWM setup more suitable in many applications, especially in a cell or engine where IRPS could not usefully be applied owing to the birefringence introduced by the windows. IRPS, however, has the unique property by which using a linear or circular polarized pump beam allows selective enhancement of the Q or R and P branches, respectively. In addition, two-dimensional images may be generated more easily using IRPS since only two laser beams are needed, and this gives it an advantage in a range of applications, especially for fundamental research.

4 Summary and conclusion

Taking acetylene and HCl as examples, the detection of trace molecules by IR-DFWM has been demonstrated using an optical device that provides stable, reliable alignment for the forward phase-matching geometry. The optical device, composed of a beam splitter plate system, overcomes one of the main difficulties that has hindered the application of DFWM in the important infrared spectral region, viz., the difficulty in aligning the two pump beams and one probe beam required for signal generation. With the present setup,

sensitivities down to 35 ppm ($\sim 9.5 \times 10^{14}$ molecules/cm^3) for C_2H_2 and 25 ppm ($\sim 6.8 \times 10^{14}$ molecules/cm^3) for HCl have been demonstrated for in situ detection with high temporal and spatial resolution in the mid-IR spectral region. Since most of the hydrocarbon molecules, e.g., CH_4, C_2H_4, and C_2H_6, and other toxic molecules, e.g., HCN and HF, have strong absorptions due to the H–M (M = C, F, Cl, CN and so on) stretching vibration in the spectral region 3000–3700 cm^{-1}, this easily aligned IR-DFWM technique has potential for wide applications to in situ detection of molecular species. In particular these species may be detected in harsh environments and at trace levels, e.g., in combustion processes, or in situations where the optical access involves transmission through windows, which would be difficult using alternative detection methods.

Acknowledgements This work was financed by the Swedish Energy Agency through CECOST (Center for Combustion Science and Technology) and VR (Swedish Research Council).

References

1. P. Ewart, S.V. O'Leary, J. Phys. B, At. Mol. Opt. Phys. **17**, 4595 (1984)
2. P. Ewart, S.V. O'Leary, Opt. Lett. **11**, 279 (1986)
3. A.C. Eckbreth, *Laser Diagnostics for Combustion Temperature and Species* (Gordon & Breach, New York, 1996)
4. R.L. Farrow, D.J. Rakestraw, Science **257**, 1894 (1992)
5. K. Kohse-Höinghaus, Progr. Energy Combust. Sci. **20**, 203 (1994)
6. K. Kohse-Höinghaus, J.B. Jeffries, *Applied Combustion Diagnostics* (Taylor & Francis, New York, 2002)
7. R.L. Vanderwal, B.E. Holmes, J.B. Jeffries, P.M. Danehy, R.L. Farrow, D.J. Rakestraw, Chem. Phys. Lett. **191**, 251 (1992)
8. G.J. Germann, D.J. Rakestraw, Science **264**, 1750 (1994)
9. G.J. Germann, R.L. Farrow, D.J. Rakestraw, J. Opt. Soc. Am. B, Opt. Phys. **12**, 25 (1995)
10. D. Voelkel, Y.L. Chuzavkov, J. Marquez, S.N. Orlov, Y.N. Polivanov, V.V. Smirnov, F. Huisken, Appl. Phys. B, Lasers Opt. **65**, 93 (1997)
11. Y. Tang, S.A. Reid, Chem. Phys. Lett. **248**, 476 (1996)
12. Y. Tang, S.A. Reid, J. Chem. Phys. **105**, 8481 (1996)
13. T.A. Reichardt, R.P. Lucht, P.M. Danehy, R.L. Farrow, J. Opt. Soc. Am. B, Opt. Phys. **15**, 2566 (1998)
14. A.C. Eckbreth, Appl. Phys. Lett. **32**, 421 (1978)
15. Z.S. Li, C.H. Hu, J. Zetterberg, M. Linvin, M. Alden, J. Chem. Phys. **127**, 084310 (2007)
16. Z.T. Alwahabi, J. Zetterberg, Z.S. Li, M. Alden, Eur. Phys. J. D **42**, 41 (2007)
17. Z.S. Li, M. Rupinski, J. Zetterberg, Z.T. Alwahabi, M. Alden, Chem. Phys. Lett. **407**, 243 (2005)
18. Z.T. Alwahabi, Z.S. Li, J. Zetterberg, M. Alden, Opt. Commun. **233**, 373 (2004)
19. Z.S. Li, Z.W. Sun, B. Li, M. Alden, M. Forsth, Opt. Lett. **33**, 1836 (2008)
20. Z.S. Li, M. Linvin, J. Zetterberg, J. Kiefer, M. Alden, Proc. Combust. Instit. **31**, 817 (2007)
21. Z.S. Li, M. Rupinski, J. Zetterberg, M. Alden, Proc. Combust. Inst. **30**, 1629 (2005)
22. K. Richard, P. Ewart, Appl. Phys. B, Lasers Opt. **94**, 715 (2009)
23. A.J. Grant, P. Ewart, C.R. Stone, Appl. Phys. B, Lasers Opt. **74**, 105 (2002)
24. R. Stevens, P. Ewart, H. Ma, C.R. Stone, Combust. Flame **148**, 223 (2007)
25. P. Lindstedt, Proc. Combust. Inst. **27**, 269 (1998)
26. H. Richter, J.B. Howard, Progr. Energy Combust. Sci. **26**, 565 (2000)
27. A. Violi, G.A. Voth, A.F. Sarofim, Proc. Combust. Inst. **30**, 1343 (2005)
28. R.L. Farrow, R.P. Lucht, W.L. Flower, R.E. Palmer, Proc. Combust. Inst. **20**, 1307 (1985)
29. R.P. Lucht, R.L. Farrow, R.E. Palmer, Combust. Sci. Technol. **45**, 261 (1986)
30. J. Bood, P.E. Bengtsson, M. Alden, Appl. Phys. B, Lasers Opt. **70**, 607 (2000)
31. G.J. Germann, A. McIlroy, T. Dreier, R.L. Farrow, D.J. Rakestraw, Ber. Bunsen-Ges.-Phys. Chem. Chem. Phys. **97**, 1630 (1993)
32. B.A. Williams, J.W. Fleming, Appl. Phys. B, Lasers Opt. **75**, 883 (2002)
33. A.V. Mokhov, S. Gersen, H.B. Levinsky, Chem. Phys. Lett. **403**, 233 (2005)
34. N. Chai, S.V. Naik, W.D. Kulatilaka, N.M. Laurendeau, R.P. Lucht, S. Roy, J.R. Gord, Appl. Phys. B, Lasers Opt. **87**, 731 (2007)
35. C.P. Rinsland, A. Baldacci, K.N. Rao, Astrophys. J. Suppl. Ser. **49** (1982)
36. R.L. Farrow, D.J. Rakestraw, T. Dreier, J. Opt. Soc. Am. B, Opt. Phys. **9**, 1770 (1992)
37. R.P. Lucht, R.L. Farrow, D.J. Rakestraw, J. Opt. Soc. Am. B, Opt. Phys. **10**, 1508 (1993)
38. B. Attal-Tretout, H. Bervas, J.P. Taran, S. LeBoiteux, P. Kelley, T.K. Gustafson, J. Phys. B, At. Mol. Opt. Phys. **30**, 497 (1997)
39. T.A. Reichardt, R.P. Lucht, J. Chem. Phys. **111**, 10008 (1999)
40. R.T. Bratfalean, G.M. Lloyd, P. Ewart, J. Opt. Soc. Am. B, Opt. Phys. **16**, 952 (1999)
41. K. Bultitude, R. Bratfalean, P. Ewart, J. Raman Spectrosc. **34**, 1030 (2003)
42. Y.B. Huang, Y.A. Yang, G.X. He, S. Hashimoto, R.J. Gordon, J. Chem. Phys. **103**, 5476 (1995)
43. S. Kim, P. Klimecky, J.B. Jeffries, F.L. Terry, R.K. Hanson, Meas. Sci. Technol. **14**, 1662 (2003)
44. D.A. Purser, *The SFPE Handbook of Fire Protection Engineering* (National Fire Protection Association, 2002)
45. A.A. Stec, T.R. Hull, K. Lebek, J.A. Purser, D.A. Purser, Fire Mater. **32**, 49 (2008)
46. I. Linnerud, P. Kaspersen, T. Jaeger, Appl. Phys. B, Lasers Opt. **67**, 297 (1998)